



Characterization of penetration induced thermal runaway propagation process within a large format lithium ion battery module



Xuning Feng^{a, b}, Jing Sun^b, Minggao Ouyang^{a, *}, Fang Wang^c, Xiangming He^{a, d},
Languang Lu^a, Hui Peng^e

^a State Key Laboratory of Automotive Safety and Energy, Tsinghua University, Beijing 100084, China

^b Department of Naval Architecture and Marine Engineering, University of Michigan, Ann Arbor, MI 48109, USA

^c China Automotive Technology and Research Center (CATARC), Tianjin 300300, China

^d Institute of Nuclear and New Energy Technology, Tsinghua University, Beijing 100084, China

^e Department of Mechanical Engineering, University of Michigan, Ann Arbor, MI 48109, USA

HIGHLIGHTS

- Thermal runaway (TR) propagation test on large format Li-ion battery pack is done.
- TR propagation mechanism in a large format Li-ion battery pack is analyzed.
- TR propagates from the nail point to the 1st battery, then to adjacent batteries.
- Side heating in TR propagation leads to a lower TR onset temperature around 100 °C.
- The heat transferred through battery shell dominates the TR propagation process.

ARTICLE INFO

Article history:

Received 26 August 2014

Received in revised form

21 October 2014

Accepted 5 November 2014

Available online 6 November 2014

Keywords:

Lithium ion battery

Safety

Thermal runaway

Thermal runaway propagation

ABSTRACT

This paper investigates the mechanisms of penetration induced thermal runaway (TR) propagation process within a large format lithium ion battery pack. A 6-battery module is built with 47 thermocouples installed at critical positions to record the temperature profiles. The first battery of the module is penetrated to trigger a TR propagation process. The temperature responses, the voltage responses and the heat transfer through different paths are analyzed and discussed to characterize the underlying physical behavior. The temperature responses show that: 1) Compared with the results of TR tests using accelerating rate calorimetry (ARC) with uniform heating, a lower onset temperature and a shorter TR triggering time are observed in a penetration induced TR propagation test due to side heating. 2) The maximum temperature difference within a battery can be as high as 791.8 °C in a penetration induced TR propagation test. The voltage responses have a 5-stage feature, indicating that the TR happens in sequence for the two pouch cells packed inside a battery. The heat transfer analysis shows that: 1) 12% of the total heat released in TR of a battery is enough to trigger the adjacent battery to TR. 2) The heat transferred through the pole connector is only about 1/10 of that through the battery shell. 3) The fire has little influence on the TR propagation, but may cause significant damage on the accessories located above the battery. The results can enhance our understandings of the mechanisms of TR propagation, and provide important guidelines in pack design for large format lithium ion battery.

© 2014 Elsevier B.V. All rights reserved.

1. Introduction

Lithium ion battery is a promising choice to power today's electric powertrains, given its high energy density and extended

cycle life. However, accidents associated with lithium ion battery failure have been reported from time to time [1–5], raising concerns and motivating research and development. The safety of lithium ion batteries, particularly associated with thermal runaway (TR) hazards, has received much attention.

The failure modes of lithium ion battery in field applications can be classified into 3 categories based on the major failure mechanism: mechanical failure, electrochemical failure and thermal

* Corresponding author.

E-mail addresses: fxn07@mails.tsinghua.edu.cn (X. Feng), ouymg@tsinghua.edu.cn (M. Ouyang).

failure [6,7]. All three modes may trigger a severe thermal hazard in a lithium ion battery system. Therefore compulsory test standards, i.e., SAE-J2464 [8], IEC-62133 [9,10], QCT-743 [11,12] and others [13–19], have been established. Safety risk still exists, although all the batteries in market can pass these test standards [20]. For example, small impurities mixed in the electrode active materials, which cannot be eliminated during the manufacture of batteries [6], may lead to short circuit defects after a long time of incubation [21] and therefore cause TR at some unpredictable point of time.

Internal short circuits (ISC) can cause severe TR of lithium ion batteries. Many researchers have studied the mechanisms of ISC [20–28] and four major approaches have been used to simulate an ISC [21]: (1) Inserting metallic particles into a battery [23]; (2) Making a battery with phase change material, which is activated at preset temperature, between the active materials [24]; (3) Indenting a battery with a blunt rod [21,25]; (4) Penetrating a battery with a nail or spike [25–28]. Nail penetration tests have long been used to simulate severe ISC induced by mechanical impact [8,11,12]. Nail penetration always leads to TR and is regarded as one of the most difficult tests for a lithium ion battery to pass.

Once a TR is initiated, TR propagation to neighboring cells is important as it can lead to violent thermal hazards. Several models have been developed to investigate TR propagation in a pack of 18,650 cells [29,30]. Simulations show that the TR propagation happens when the triggering battery is in good contact with others [29]. Experimental data is analyzed for the TR propagation behavior in a pack of 18650 cells [31]. However, little model validation work has been done.

For TR research, large format batteries are of special interest. On one hand, large format helps to reduce the number of cells, thereby reducing system complexity [32]. On the other hand, a large format battery is more vulnerable to TR because it contains more stored energy and has larger variation in its temperature distribution. A hot spot can cause local meltdown of the separator, leading to ISC. ISC could propagate to the whole battery resulting in a severe thermal hazard [33]. For large format lithium ion batteries, a TR model for a single cell was established a few years ago [33,34], followed by a model for TR propagation within a battery pack [35]. However, experimental validation has not been provided in literature to the best knowledge of the authors.

The goal of this paper is to analyze the mechanisms of a penetration-induced TR propagation within a large format lithium ion battery module, including both TR initiation and propagation processes to understand the mechanisms and gain insights to the thermal hazards of a battery pack system. The TR behavior of single battery is based on the work reported in Refs. [36,37]. In our experiments, the TR was triggered by nail penetration of the first battery, which might trigger TR propagation to subsequent batteries. Temperature distribution and voltage variation were used to characterize the mechanisms of TR propagation. Moreover, the physical damages caused by TR propagation were analyzed by disassembling the battery module after experiments. We choose $\text{LiNi}_x\text{Co}_y\text{Mn}_z\text{O}_2$ (NCM) as the cathode of the battery because NCM cathode material demonstrates higher capacity, good thermal stability and lower toxicity among the family of Li-ion batteries [6,38,39].

2. Experiments

2.1. The battery

The 25Ah battery used in this paper is manufactured by the AE Energy Co. Ltd. with NCM/graphite as its electrodes [36,37]. The battery consists of two pouch cells in an aluminum shell, which are connected in parallel, as shown in Fig. 1a. A micro-thermocouple

was inserted between the two pouch cells to measure the internal temperature of the battery.

Six batteries formed a battery module in a penetration induced TR propagation test. Fig. 1b shows the definitions of cell, battery and battery module in this paper. To avoid misunderstanding, we call the two pouch cells “cell” and the battery cell “battery” in the following sections. In other words, two cells formed a battery, and six batteries formed a battery module.

2.2. EV-ARC test of a battery

The battery was heated into TR using an extended volume-accelerating rate calorimetry (EV-ARC), as reported in Ref. [36]. An EV-ARC test follows the heat-wait-seek method and provides an adiabatic calorimetric environment for thermal analysis. The EV-ARC test result is used for further analysis in this paper. Fig. 2 shows the EV-ARC used in Refs. [36,37] and this paper.

2.3. Thermal runaway propagation tests of battery modules

Penetration induced TR propagation tests on a battery module were conducted using the penetration test bench (Fig. 3a) inside an explosion-proof room at the Battery Test Laboratory of China Automotive Technology and Research Center (CATARC). Six batteries were clamped together using two pieces of steel holder, as illustrated in Fig. 3b. Bat i ($i \in \{1,2,3,4,5,6\}$) is used to describe the i th battery towards the direction where the nail came in, e.g., Bat 1 was penetrated by the nail, while Bat 2 was heated to TR by Bat 1. Kapton tape of 0.6 mm thickness was used to wrap the batteries to avoid short circuits through the shell and to hold the thermocouples. Thermal resistant layers (made by asbestos) were inserted between the battery module and the steel holder to avoid excessive heat transfer to the holder.

Given the explosive nature of the testing, extra care had been paid to assure safety of the people and equipment involved. Cameras were employed to monitor the experiment so that the testers could stand outside the explosion-proof room to guarantee safety. Disassembling work after tests was performed after the toxic gases were exhausted by the air-blower inside the explosion-proof room.

Three tests were performed under different settings, as listed in Table 1. For experiment No. 1 and No. 2, the batteries were connected in series using connectors, while for experiment No. 3 the batteries were not connected. The battery voltage was monitored, and flame retardant layers were introduced to protect the voltage monitoring circuit from fire for experiment No. 2 and 3 but not for experiment No. 1.

47 Thermocouples ($\text{TC}_1\text{--TC}_{47}$) were placed at selected points within the battery module, as marked in Fig. 3b and summarized in Table 2. The internal temperature of the batteries were monitored by inserting $\text{TC}_1\text{--TC}_8$ inside the battery as described in Fig. 1. $\text{TC}_1\text{--TC}_6$ were placed at the center of each battery. In addition, two more TCs were placed inside Bat 1 (TC_7) and Bat 2 (TC_8) 20 mm away from the center to observe the temperature difference away from the battery core. The pole temperatures were monitored using $\text{TC}_9\text{--TC}_{18}$. $\text{TC}_{19}\text{--TC}_{29}$ were placed on plane A (in red in the web version) and plane C, while $\text{TC}_{30}\text{--TC}_{47}$ were located on plane B (in blue), as well as at the centers of the battery surfaces. $\text{TC}_{19}\text{--TC}_{47}$ were used to analyze the temperature distribution within a battery.

Bat 1 was penetrated using a nail with 8 mm diameter at a speed of 10 mm/s. After Bat 1 was penetrated, TR propagated to adjacent batteries sequentially, as shown in Fig. 4. The TR propagation behavior, including the temperature and voltage responses, will be described in the following sections.

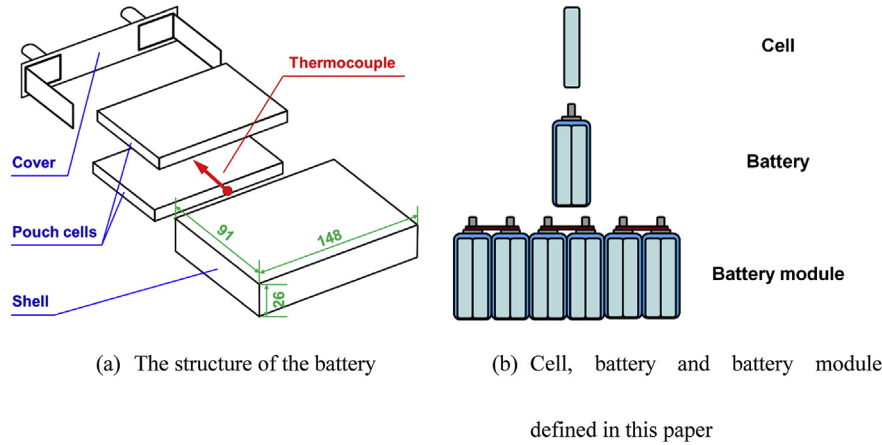


Fig. 1. The cell, battery and battery module.



Fig. 2. Picture of the EV-ARC used in this research.

3. Results and discussions

3.1. Overview

Fig. 4 shows the core temperature (solid line) and the temperature between the batteries (dotted line) for all of the three experiments.

The onset time $t_{\text{onset},i}$ and onset temperature $T_{\text{onset},i}$ for TR of Bat i are defined by (1) and (2), respectively. We also use t_{onset} and T_{onset} to represent $t_{\text{onset},i}$ and $T_{\text{onset},i}$ in general without specific designation to i . k indicates the time index of the data, which was recorded with a sampling time of 1 s. Additionally, TR propagation time, $D_{i,i+1}$, can be calculated from (3).

$$t_{\text{onset},i} = \min\{k : TC_i(k+1) - TC_i(k) > 10^\circ\text{C}\}, \quad i \in \{1, 2, 3, 4, 5, 6\} \quad (1)$$

$$T_{\text{onset},i} = TC_i(t_{\text{onset},i}), \quad i \in \{1, 2, 3, 4, 5, 6\} \quad (2)$$

$$D_{i,i+1} = t_{\text{onset},i+1} - t_{\text{onset},i}, \quad i \in \{1, 2, 3, 4, 5\} \quad (3)$$

Table 3 reports $T_{\text{onset},i}$ for all the experiments. $T_{\text{onset},i}$ was in a range of 65–116 °C. Table 4 reports $D_{i,i+1}$, for all of the experiments. The values of $D_{i,i+1}$ were close for different i except for $D_{1,2}$, which shows that it took longer time for TR to propagate from Bat 1 to Bat 2.

The maximum temperature for Bat i , $T_{\text{max},i}$, is defined in (4). And the moment when $T_{\text{max},i}$ occurs, $t_{\text{max},i}$, is defined in (5), where ‘argmax’ means the ‘argument of the maximum value’, namely the value of the variable at which the function takes the maximum value, as a standard notation used in optimization [40].

$$T_{\text{max},i} = \max_k \{TC_i(k)\}, \quad i \in \{1, 2, 3, 4, 5, 6\} \quad (4)$$

$$t_{\text{max},i} = \arg \max_k \{TC_i(k)\}, \quad i \in \{1, 2, 3, 4, 5, 6\} \quad (5)$$

Table 5 compares the maximum temperature for Bat i , $T_{\text{max},i}$, during the penetration induced TR propagation tests. The range of $T_{\text{max},1}$ for the penetrated Bat 1 (764–862 °C) was lower than that of Bat 2–6 (873–930 °C).

3.2. Thermal runaway propagates from the penetration point to the 1st battery

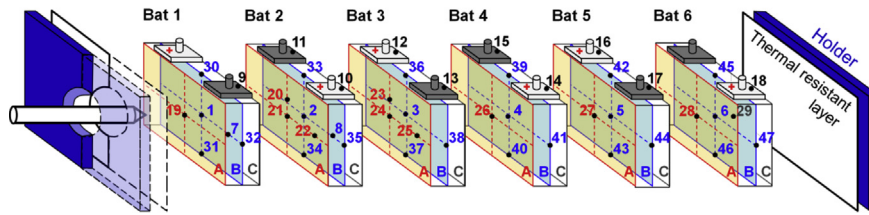
TR propagated from the penetration point to Bat 1 after the penetration, as illustrated in Fig. 5a. It took less than 5 s for the TR to propagate from the location of TC_1 to that of TC_7 , which was 20 mm from TC_1 . However, about 10 s after the TR was triggered, the temperature recorded by TC_1 was lower than TC_7 as shown in Fig. 5b, because the nail inside Bat 1 provided a heat sink to absorb TR heat.

3.3. Thermal runaway propagates to adjacent batteries

TR propagated from Bat 1 to Bat 2 after the TR of Bat 1. The TR propagation process was driven by the large temperature difference between Bat 1 and Bat 2. Fig. 6 collects all the temperature data for Bat 2 of experiment No. 1. As shown in Fig. 6a, when TR was triggered in Bat 1, the temperature at the front edge of Bat 2 (blue lines in the web version) rose first and formed a temperature gradient for heat transfer, which led Bat 2 to TR (red lines) and thereby raised the temperature at its back (green lines) and heated up Bat 3.



(a) Test setup



(b) Thermocouple locations

Fig. 3. Experimental setup of the penetration induced TR propagation tests.

Table 1
Experiment settings.

Experiment no.	Connected in series?	Voltage monitoring circuit protected by flame retardant layer?
1	Y	N
2	Y	Y
3	N	Y

Table 2
Thermocouple locations.

Measurement	Thermocouple (TC) no.
Core temperature	1–8
Pole temperature	9–18
Temperature on plane A/C	19–29
Temperature on plane B, at the surface center.	30–47

3.4. The maximum temperature difference within a battery

The maximum temperature difference for Bat i (MTD_i) is defined by (6) to quantify the non-uniformity of the temperature distribution, where k is the time index, and m and n are the indices of the thermocouples placed on Bat i . The maximum value of MTD_i , $MTD_{max,i}$, is defined by (7) as an indicator of temperature non-uniformity for the large format battery.

$$MTD_i(k) = \max_{m,n} \left\{ \left| TC_m(k) - TC_n(k) \right|, m, n \in \text{Bat } i \right\} \quad (6)$$

Table 3
Onset temperature of TR, $T_{onset,i}$ [°C].

Exp. No.	$T_{onset,1}$	$T_{onset,2}$	$T_{onset,3}$	$T_{onset,4}$	$T_{onset,5}$	$T_{onset,6}$
1	Ambient temperature	78	65	75	79	77
2	Ambient temperature	116	74	86	86	71
3	Ambient temperature	74	66	80	106	73

Table 4
TR propagation time, $D_{i,i+1}$ [s].

Exp. No.	$D_{1,2}$	$D_{2,3}$	$D_{3,4}$	$D_{4,5}$	$D_{5,6}$
1	245	163	186	164	159
2	481	161	156	157	137
3	210	164	183	181	113

Table 5
 $T_{max,i}$ [°C] when TR happens.

Exp. No.	Bat 1	Bat 2	Bat 3	Bat 4	Bat 5	Bat 6
1	832	885	930	883	889	873
2	764	884	924	920	912	905
3	862	877	911	909	906	897

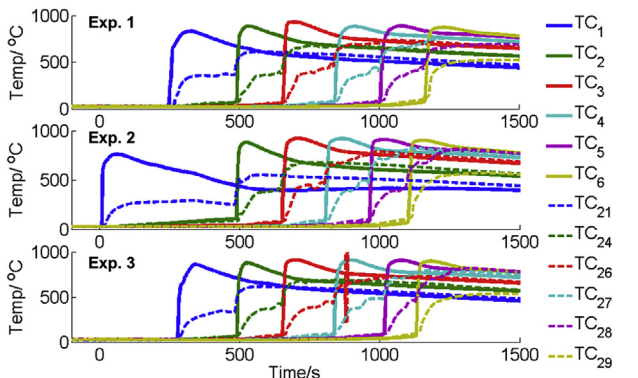


Fig. 4. Temperature responses of three penetration induced TR propagation tests, TCs in the legend mean thermocouple and their subscripts can be referred in Fig. 3b.

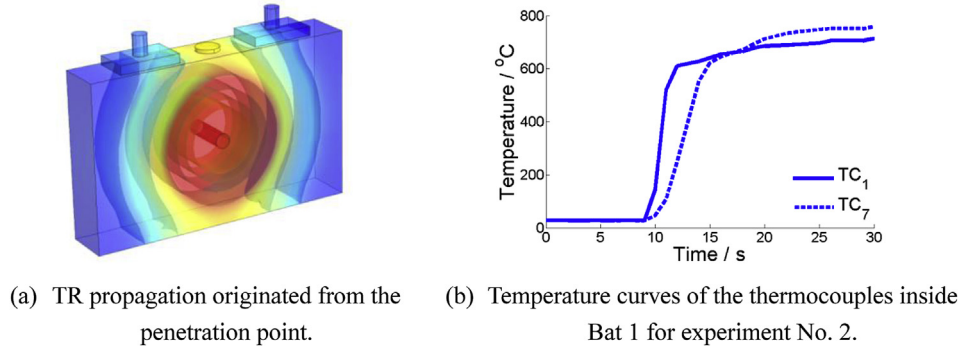


Fig. 5. Illustration of the TR propagation within the 1st battery.

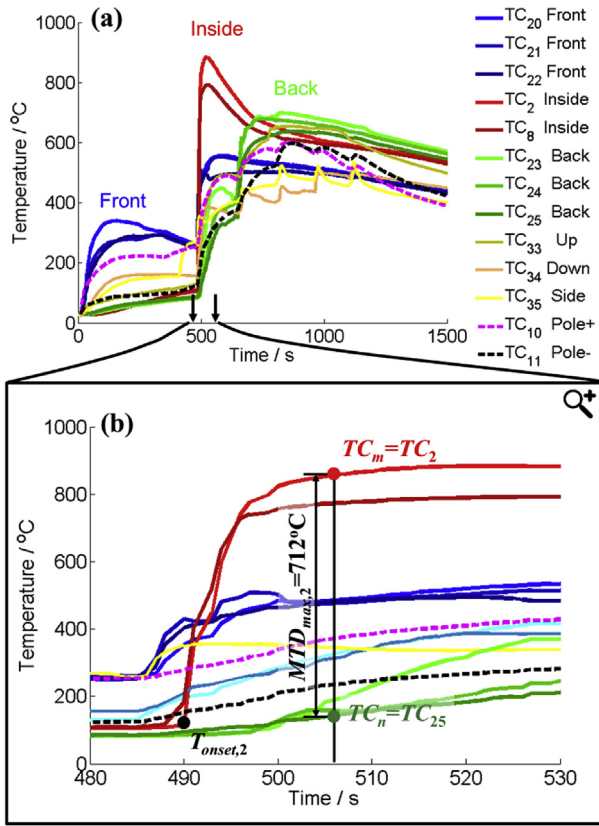


Fig. 6. Temperature of the thermocouples placed on Bat 2 in experiment No. 1.

$$MTD_{max,i} = \max_k \{ MTD_i(k) \} \quad (7)$$

Fig. 6b illustrates the definition of $MTD_{max,i}$ for Bat 2 in experiment No. 1. $MTD_{max,2}$ in Fig. 6b was 712 °C. When $MTD_{max,2}$ occurred, the maximum temperature was reported by $TC_m = TC_2$, while the minimum temperature by $TC_n = TC_{25}$. Table 6 compares

Table 6
 MTD_{max} [°C] of three experiments.

Exp. No.	Bat 1	Bat 2	Bat 3	Bat 4	Bat 5	Bat 6
1	630	712	792	624	648	593
2	680	714	712	766	718	703
3	693	695	762	679	711	707

$MTD_{max,i}$ for all the experiment results. $MTD_{max,i}$ was in a range of 593–792 °C, which is higher than 523–553 °C as reported in EV-ARC test in Ref. [36].

Table 7 collects thermocouple indices (m, n in Eq. (6)) corresponding to the hottest and the coolest locations at the moment when the $MTD_{max,i}$ occurred. Referring to Fig. 3b, the results show that the maximum temperature, TC_m , always occurred at the center of the battery, while the minimum temperature, TC_n , always occurred at the back surface of the battery.

3.5. The difference between the uniform heating in an EV-ARC test and side heating in a penetration induced TR propagation test

Some critical TR characterizations of the penetration induced TR propagation test are different from those of the EV-ARC test. The differences have been compared to help reveal the TR propagation mechanism.

The battery tested by EV-ARC was heated inside a chamber with uniform temperature distribution, as illustrated in Fig. 7a. The maximum temperature difference within the battery does not exceed 1 °C for 97% of the time during an EV-ARC test [36]. Fig. 7b shows the temperature curve of an EV-ARC test: the maximum temperature (T_{max}) is 854 °C, while the onset temperature ($T_{onset,ARC}$) is 259 °C. It took about 189,767 s for the battery to go from ambient temperature to TR, which is named as D_{ARC} .

In a penetration induced TR propagation test, side heating brought Bat 2–6 into TR, as shown in Fig. 7c. The maximum temperature difference ($MTD_{max,i}$) within the battery can be 593–792 °C as reported in Sec. 3.4. Fig. 7d shows the internal temperature (TC_2) of Bat 2 in experiment No. 1: the maximum temperature ($T_{max,2}$) was 885 °C, while the onset temperature ($T_{onset,2}$) was 78 °C. It took about 245 s for TR to propagate from Bat 1 to Bat 2.

Table 8 compares the key results of the penetration induced TR propagation test in this paper with that of the EV-ARC test. The maximum temperatures (T_{max}) in the EV-ARC test and in the penetration induced TR propagation test were very similar. However, the propagation duration $D_{i,i+1}$ was less than 1% of D_{ARC} .

Table 7
Thermocouple indexes m and n defined in (6) when $MTD_{max,i}$ occurred.

Exp. no.	Bat 1		Bat 2		Bat 3		Bat 4		Bat 5		Bat 6	
	m	n										
1	1	20	2	25	3	26	4	27	5	28	6	29
2	7	20	2	25	3	26	4	27	5	28	6	29
3	7	20	8	24	3	26	4	40	5	28	6	29

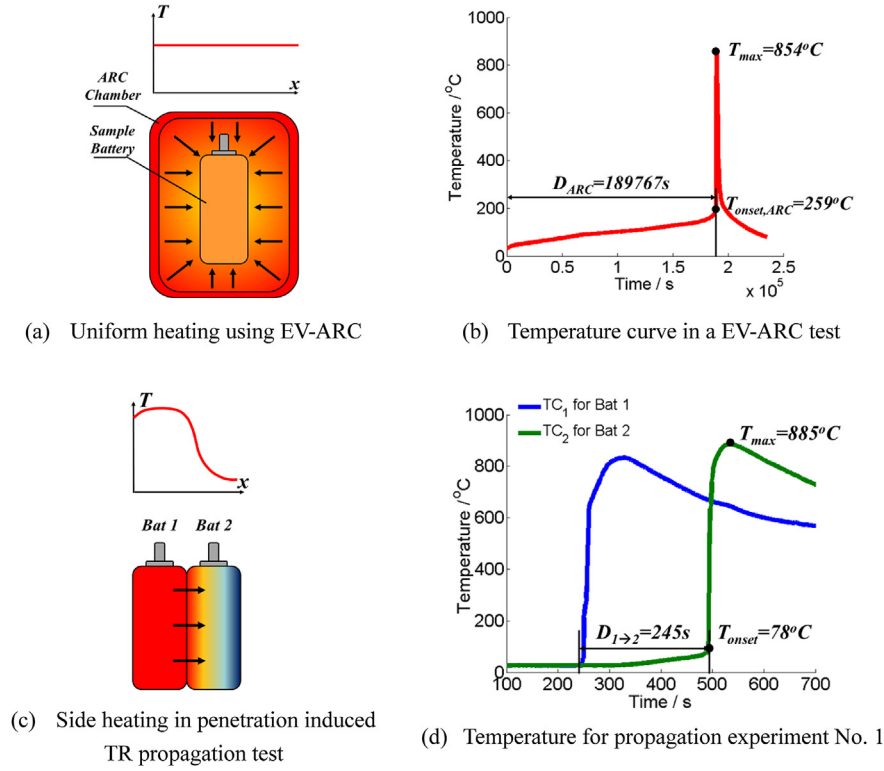


Fig. 7. Comparison of the uniform heating and side heating.

indicating the TR propagation was quite fast from one battery to its neighbor.

Furthermore, $T_{\text{onset},i}$ in the penetration induced TR propagation test was much lower than $T_{\text{onset,ARC}}$, and the reason can be explained by Fig. 8 and Fig. 9 through a thermal resistance network analysis. In the EV-ARC test, the temperature distribution is quite uniform before TR happens, as discussed in Ref. [36]. Therefore only when the whole battery temperature rises to the onset temperature limit, $T_{\text{onset,ARC}} = 259^\circ\text{C}$, does TR happen. It is believed that $T_{\text{onset,ARC}}$ is the temperature when the separator collapses and serious internal short circuit (ISC) occurs [36]. In a penetration induced TR propagation test, however, the temperature distribution is not uniform due to side heating and thermal resistance between adjacent batteries.

Given the internal temperature of Bat i and $i + 1$, whose profiles are shown in Fig. 4, the temperature distributions between the two nodes can be determined for different stages of TR propagation according to heat transfer theory [41]. The red (blue) dot in the web version in Fig. 8 represents the internal temperature of Bat i (Bat $i + 1$), or TC_i (TC_{i+1}). The total thermal resistance between TC_i and TC_{i+1} , R , can be calculated from Eq. (8), where R_{jr} , $R_{\text{Ap},1}$, $R_{\text{Ap},2}$, R_{shell} and R_K represent the thermal resistance of the jelly roll, the outer Al-plastic film, the inner Al-plastic film, the battery shell and the Kapton tape, respectively (Fig. 8).

$$R = 2 \times (R_{\text{jr}} + R_{\text{Ap},1} + R_{\text{Ap},2} + R_{\text{shell}} + R_K) \quad (8)$$

T_Δ , the temperature for the thermocouple located between the two batteries, marked by a yellow triangle in Fig. 8, can be interpolated by Eq. (9), where α is the proportion factor for the thermal resistance within Bat $i + 1$, defined in Eq. (10). In this case, to fit the dotted curve in Fig. 4, the range of α should be $0.4 < \alpha < 0.5$.

$$T_\Delta = TC_{i+1} + \alpha \cdot (TC_i - TC_{i+1}) \quad (9)$$

$$\alpha = \frac{R_{\text{shell}} + R_{\text{Ap},1} + R_{\text{jr}} + R_{\text{Ap},2}}{R} \quad (10)$$

Furthermore, T_\diamond , the temperature at the front edge of Bat $i + 1$'s jelly roll (marked by the yellow diamond in Fig. 8) is critical in determining the onset of TR for Bat $i + 1$. In other words, when T_\diamond equals $T_{\text{onset,ARC}}$, the separator at the front edge of Bat $i + 1$ collapses and internal short circuit induced TR occurs at Bat $i + 1$, Eq. (11). T_\diamond can be interpolated by Eq. (12), where β is the proportion factor for the sum of R_{jr} and $R_{\text{Ap},2}$ (Eq. (13)). To match Eq. (11) in Fig. 9c, β is set as 0.25.

$$T_\diamond(t_{\text{onset},i+1}) = T_{\text{onset,ARC}} \quad (11)$$

$$T_\diamond = TC_{i+1} + \beta \cdot (TC_i - TC_{i+1}) \quad (12)$$

$$\beta = \frac{R_{\text{jr}} + R_{\text{Ap},2}}{R} \quad (13)$$

Fig. 9a–d shows the temperature distributions of two adjacent batteries, at different stages during TR propagation, calculated by Eqs. (8)–(13). Fig. 9a shows that when $t = t_{\text{max},i}$, TR happens at Bat i and TC_i rises to its highest value. T_Δ is higher than the TR onset temperature $T_{\text{onset,ARC}}$, while T_\diamond is lower than $T_{\text{onset,ARC}}$. Fig. 9b shows that as time goes on, TC_i drops because of heat dissipation, while TC_{i+1} rises slowly. Fig. 9c shows that at $t = t_{\text{onset},i+1}$, T_\diamond reaches the critical value of $T_{\text{onset,ARC}}$, leading to TR of Bat $i + 1$, when the core temperature TC_{i+1} is much lower than $T_{\text{onset,ARC}}$. That explains why $T_{\text{onset},i} = 65\text{--}116^\circ\text{C} < T_{\text{onset,ARC}}$ as shown in Table 8. Fig. 9d illustrates that after a few seconds, the core temperature TC_{i+1} rises to its highest value and Bat $i + 1$ is heating Bat $i + 2$. In

Table 8
Comparison of critical results in EV-ARC test and module penetration test.

	The EV-ARC test results [36]	Propagation test results
Maximum temperature/ $^{\circ}\text{C}$	$T_{\max} = 854$	$T_{\max,i} = 873\text{--}930, i \in \{2,3,4,5,6\}$
TR duration/s	$D_{\text{ARC}} = 189767$	$D_{1,2} = 210\text{--}481$; $D_{i,i+1} = 113\text{--}186, i \in \{2,3,4,5\}$.
Onset temperature/ $^{\circ}\text{C}$	$T_{\text{onset,ARC}} = 259$	$T_{\text{onset},i} = 65\text{--}116, i \in \{2,3,4,5,6\}$.

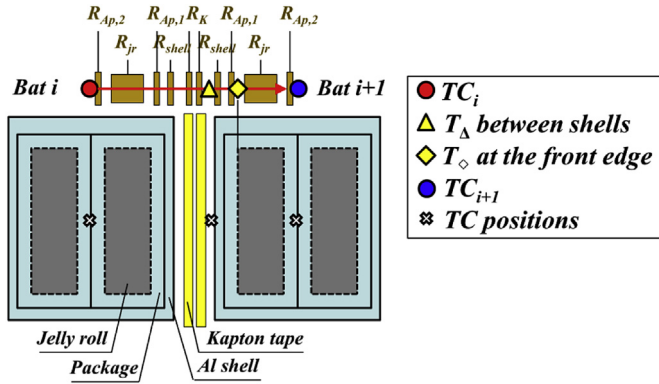


Fig. 8. Thermal resistance between adjacent batteries.

summary, Fig. 9 explains that a lower onset temperature and shorter TR triggering time in a penetration induced TR propagation test is caused by side heating.

3.6. Voltage variation

Fig. 10 reports the voltage responses for the penetration induced TR propagation tests. Note that external short circuit caused by fire, which is common in battery safety tests [42], occurred in the voltage curve for Bat 4, 5 and 6 in experiment No. 1 and for Bat 4 and 5 in experiment No. 3. The voltage data corresponding to those batteries are excluded in our further analysis.

Voltage curves without short circuit events can be divided into 5 stages corresponding to different phases in physical/chemical process. Fig. 11a shows the 5-stage voltage profile for Bat 3 in experiment No. 1, where t_j and V_j ($j \in \{1,2,3,4,5\}$) represent the start time and voltage of Stage j , respectively. Table 9 describes the features of the 5-stage voltage profile at each stage. Note that the battery is composed of two pouch cells inside as shown in Fig. 1, which will be referred to as the front and back pouch cell respectively as shown in Fig. 11b.

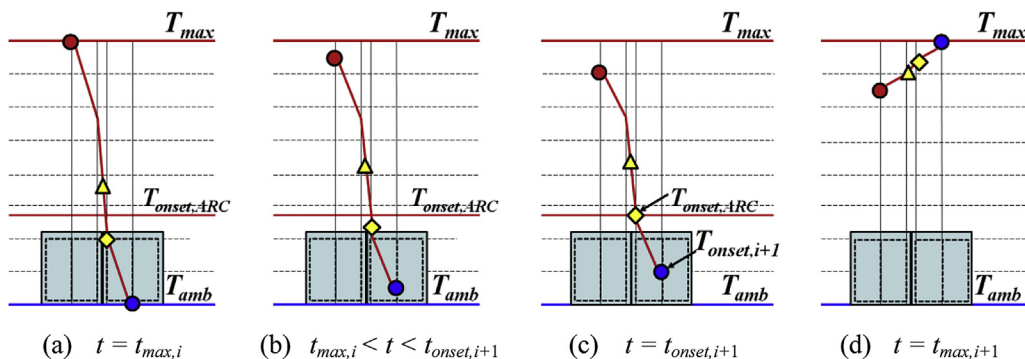


Fig. 9. Temperature distribution at different stages of TR propagation.

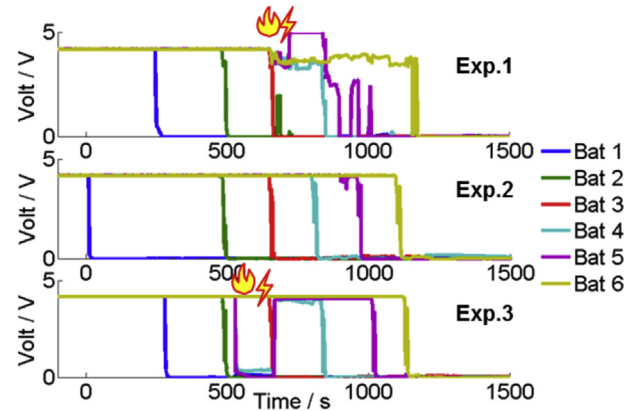


Fig. 10. Voltage results and fire induced short at the voltage monitoring circuits.

The 5-stage voltage profile fitted almost all the Bat i for $i \in \{2, 3, 4, 5, 6\}$, except those suffered external short circuits as shown in Fig. 10. Therefore we have 10 samples to acquire the statistics of V_i , as listed in Table 10. V_{in} indicates the initial voltage of the batteries before a module penetration test as a reference. Large values in standard deviation of V_3 (the valley point), and V_4 (the rebound point) reflect the effects of uncertainties associated with the conditions when the front and back pouch cells were disconnected.

Moreover, as shown in Fig. 11a, T_{onset} is always reached later than t_2 , which is the start of the quick voltage drop. The delay from the voltage drop to the temperature rise indicated the time it took for the heat transfer from the core of the pouch cell to its surface. Such a time delay was also reported in an EV-ARC test [36].

3.7. The fire on the top of the battery module

The material blowout causes about 28% loss in mass for the battery that went through the TR process. The electrolyte, which accounts for 15% of the total mass of the battery [37], burst out and brought out another 13% of the battery materials with them. The burst out electrolyte was ignited, which led to the fire scorching the covers of adjacent batteries.

However, it is hard to predict the occurrence of fire, since we have observed TRs both with and without fire for different batteries. No fire but smoke was observed when Bat 1 and 2 ran into TR in experiment No. 1, while fire could be observed every other time when a battery ran into TR, as shown in Fig. 12 and Table 11. Fig. 13 displays the cover temperature for the penetration induced TR propagation tests. When there was no fire when a battery ran into TR (Bat 1 and 2 in experiment No.1), one could observe that there

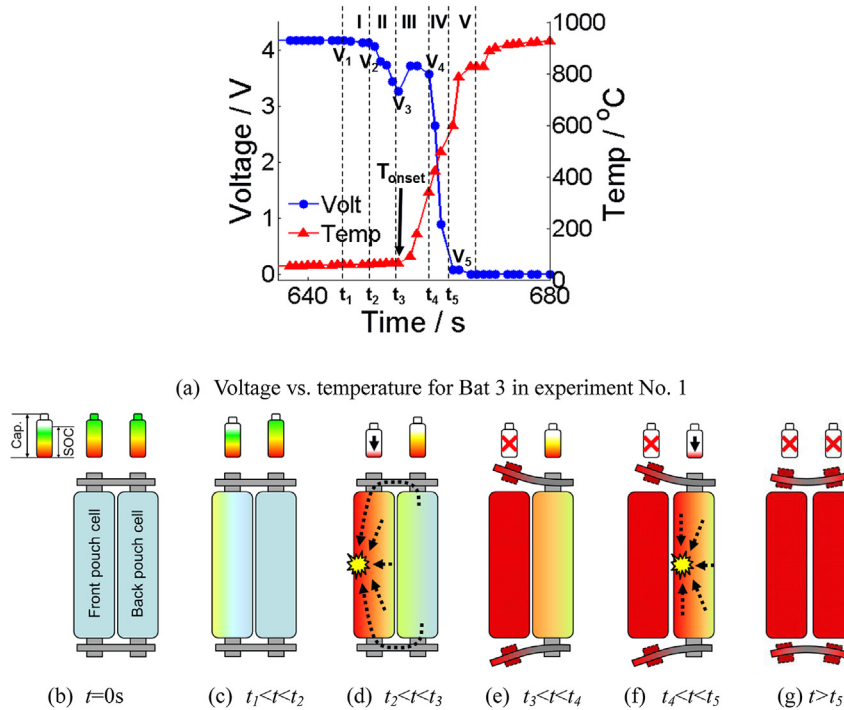


Fig. 11. Characterization of voltage response stages (result of Bat 3 in experiment No. 1).

was no obvious temperature increase in the cover of adjacent batteries (Bat 2 and 3 in experiment No.1 in Fig. 13). Pulses can be clearly seen in the temperature profiles for experiment No. 2, as a result of the venting process with fire. However, such pulses are not always observable for every battery that was exposed to fires when its neighbor went through TR. In addition, temperature plateaued at about 150 °C, which is the temperature at the inner cone (the bottom of the flame), indicating that the fire caused by the TR of Bat i was scorching the covers of Bat $i + 1$.

3.8. Heat transfer paths

The heat released in TR can be transferred through the battery shell, through the pole connector as well as by fire scorching on the

top of the batteries, as illustrated in Fig. 14a. The burst out electrolyte caught fire on top of the battery, which scorched adjacent batteries. The heat flow transferred from Bat i to Bat $i + 1$ through the three paths can be calculated by (14), where R_x is the thermal resistance between the temperature nodes TC_y and TC_z , as shown in Fig. 14b. R_x can be calculated according to the second column of Table 12, where λ_x is the thermal conductivity, δ_x is the heat transfer distance and A_x is the area that the heat flow passes. The subscript x used in the Eqs (14)–(16) can be s , p or f , where s stands for the battery shells, p for the pole connectors, and f for the fire scorching on the cover. As listed in Table 12, λ_x is acquired from Refs. [41,43], while A_x is calculated according to the geometry of the battery.

$$q_{x,i}(t) = \frac{TC_y(t) - TC_z(t)}{R_x}, \quad \left(x \in \{s, p, f\}, i \in \{1, 2, 3, 4, 5\} \right) \quad (14)$$

Let y and z denote the indices of the thermocouple located at the start and the end point of the heat transfer. As listed in Table 13, when $x = s$, $TC_y = TC_i$ and $TC_z = TC_{i+1}$ are the core temperature of Bat i and Bat $i + 1$, respectively; when $x = p$, TC_y and TC_z refer to the thermocouple located at the negative pole of Bat i and at the positive pole of Bat $i + 1$, respectively; when $x = f$, TC_y and TC_z refer to the temperature at the battery cover (which is also the temperature at the bottom of flame) and the core temperature of Bat $i + 1$, respectively.

Fig. 15 shows the temperature profiles (TC_y and TC_z) that are used for heat transfer analysis: Fig. 15a shows the core temperatures; Fig. 15b shows the pole temperatures; Fig. 15c shows the

Table 9
Descriptions of the 5-stage voltage profile.

Stage	Description
I	When the core temperature of the battery rose to 50 °C or higher, the voltage started to drop slowly from V_1 because of high temperature degradation as discussed in Refs. [36,37], Fig. 11c.
II	The voltage drop accelerated from V_2 , indicating that serious short circuit had occurred. When the front edge of the front pouch cell was heated to $T_{\text{onset_ARC}}$, the separator collapsed and therefore the short circuit happened at the front edge of the front pouch cell which led to TR. Some of the electric energy of the back pouch cell was also released at this time, as the two pouch cells were connected in parallel, Fig. 11d.
III	The voltage rebounded from V_3 to V_4 for about 5 s. Fig. 11e shows the reason for the voltage rebound in Stage III. High temperature brought by TR broke the electric connection between the two pouch cells, when the back pouch cell was not fully discharged. Therefore V_4 represents the voltage of the back pouch cell in Stage III.
IV	The voltage dropped quickly indicating the short-circuit-induced TR of the back pouch cell, Fig. 11f.
V	The voltage leveled to a value lower than 1 V, indicating the end of electro-chemical reaction during TR. Finally, both of the two pouch cells went into TR, Fig. 11g.

Table 10
Statistics of the critical voltages for the 5-Stage voltage profile.

	V_{in}	V_1	V_2	V_3	V_4	V_5
Average value/V	4.166	4.159	4.115	1.940	3.352	0.247
Standard deviation/V	0.006	0.015	0.042	1.070	0.651	0.125

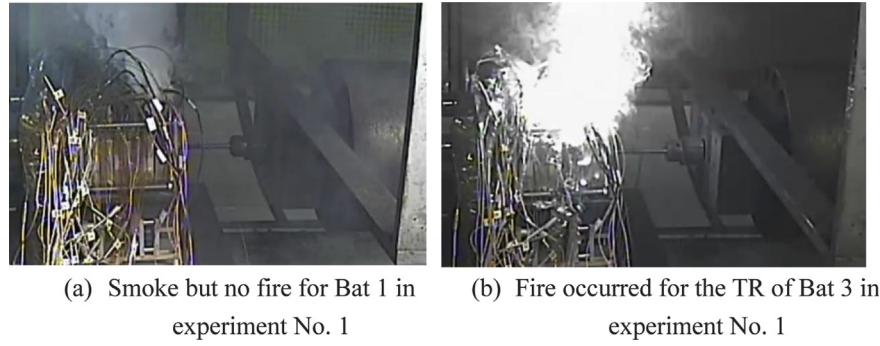


Fig. 12. Illustration of the unpredictable fire, screen shot of the monitoring video during penetration induced TR propagation test.

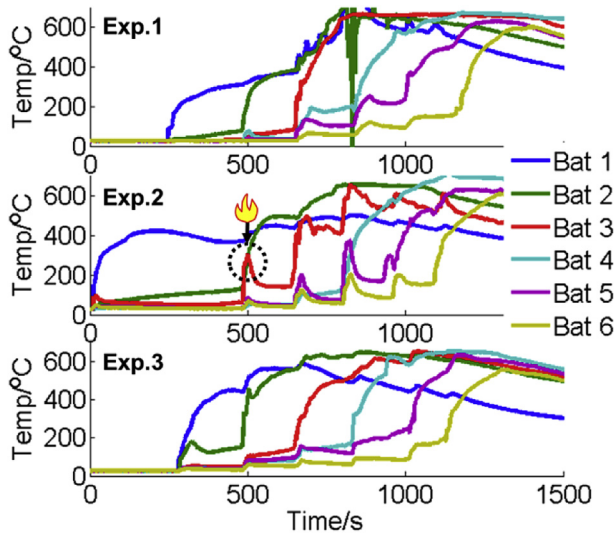


Fig. 13. The cover temperatures during penetration induced TR propagation test.

Table 11
Fire or not during penetration induced TR propagation test.

Exp. no.	Bat 1	Bat 2	Bat 3	Bat 4	Bat 5	Bat 6
1	Smoke but no fire	Smoke but no fire	Fire	Fire	Fire	Fire
2	Fire	Fire	Fire	Fire	Fire	Fire
3	Fire	Fire	Fire	Fire	Fire	Fire

cover temperatures vs. the core temperatures. The shaded area in Fig. 15 represents the integration of temperature difference, which is proportional to the total heat transferred during TR propagation, defined as $Q_{x,i}$. $P_{x,i}(t)$ is the total heat transferred from Bat i to Bat $i+1$ at time t , as defined in (15), where $t_{onset,i}$ indicates the TR onset time for Bat i . When t equals $t_{onset,i+1}$, $Q_{x,i}$ equals $P_{x,i}(t)$ as defined in Eq. (16). For example, if we focus on Bat 1, we can get $Q_{s,1} = 68,881$ J from Fig. 15a, $Q_{p,1} = 14,586$ J from Fig. 15b and $Q_{f,1} = 162$ J from Fig. 15c.

$$P_{x,i}(t) = \int_{t_{onset,i}}^t q_{x,i}(\tau) d\tau, \quad i \in \{1, 2, 3, 4, 5\} \quad (15)$$

$$Q_{x,i} = P_{x,i}(t = t_{onset,i+1}) = \int_{t_{onset,i}}^{t_{onset,i+1}} q_{x,i}(\tau) d\tau, \quad i \in \{1, 2, 3, 4, 5\} \quad (16)$$

The total TR heat released in an EV-ARC test, ΔH , can be calculated using Eq. (17), according to the data provided in Table 5 of [36], where $M = 0.72$ kg is the mass of the battery, $C_p = 1100$ J kg⁻¹ K⁻¹ is the measured heat capacity and $\Delta T = 854 - 90 = 764$ °C is the temperature difference between the maximum temperature (854 °C) and the onset temperature (90 °C) of self-heating.

$$\Delta H = M \cdot C_p \cdot \Delta T = 605088 \text{ J} \quad (17)$$

Table 14 compares the normalized heat transfer ratios, $Q_{s,i}/\Delta H$, $Q_{p,i}/\Delta H$ and $Q_{f,i}/\Delta H$ in penetration induced TR propagation tests. The heat transfer caused by fire is very small according to our calculation. The fact that there is no obvious difference in the TR

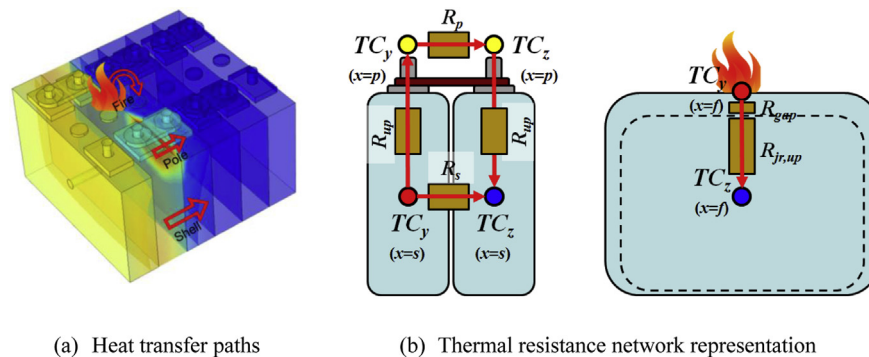


Fig. 14. Heat transfer paths during thermal runaway propagation.

Table 12
Physical parameters used in heat transfer calculation.

x	R_x	$\lambda_x/W\ m^{-1}\ K^{-1}$	δ_x/m	A_x/m^2
s	$R_s = \frac{\delta_s}{\lambda_s \cdot A_s}$	0.5 [43]	0.026	0.01354
p	$R_p = \frac{\delta_p}{\lambda_p \cdot A_p}$	146 (Brass 300 °C [41])	0.026	0.00004
f	$R_f = R_{f,up} + R_{gap}$	$R_{f,up} = \frac{\delta_{f,up}}{\lambda_{f,up} \cdot A_f}$ $R_{gap} = \frac{\delta_{gap}}{\lambda_{gap} \cdot A_f}$	20 [43] 0.014 (Air 150 °C [41])	0.043 0.00385

Table 13
Thermocouple indices for (y, z).

x		$i = 1$	$i = 2$	$i = 3$	$i = 4$	$i = 5$
s	y	1	2	3	4	5
	z	2	3	4	5	6
p	y	9	11	13	15	17
	z	10	12	14	16	18
f	y	33	36	39	42	45
	z	2	3	4	5	6

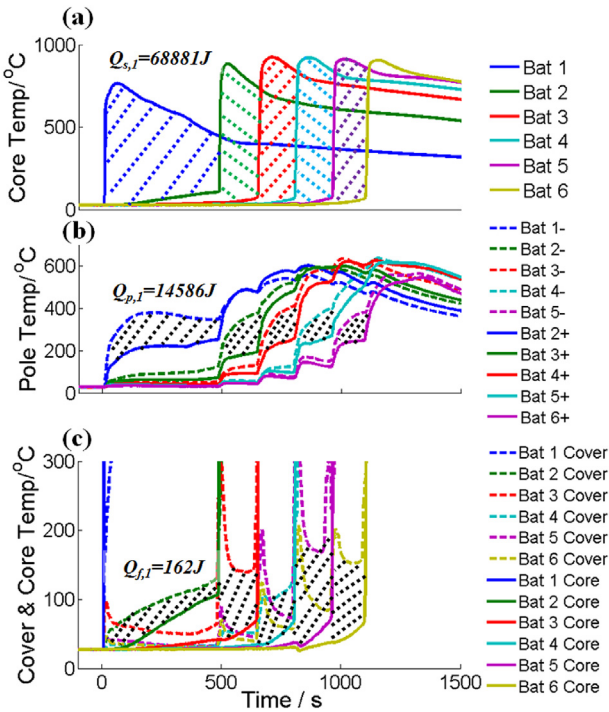


Fig. 15. Heat transfer through the shell and through the connector.

propagation duration $D_{i,i+1}$ (Table 4) for those batteries with and without fire (Table 11) proves that the fire has little influence on the TR propagation process. However, it must be taken seriously that the fire may lead to secondary thermal hazards on the accessories

Table 14
Normalized heat transfer ratios for different heat transfer paths.

Exp. no.	$Q_{x,i}/\Delta H$	$i = 1$	$i = 2$	$i = 3$	$i = 4$	$i = 5$
1	$Q_{s,i}/\Delta H$	7.3%	5.5%	6.4%	5.4%	5.4%
	$Q_{p,i}/\Delta H$	1.2%	0.60%	1.1%	0.56%	0.65%
	$Q_{f,i}/\Delta H$	0.0063%	0.0076%	0.042%	0.050%	0.027%
2	$Q_{s,i}/\Delta H$	11.4%	5.3%	5.4%	5.5%	4.8%
	$Q_{p,i}/\Delta H$	2.4%	0.87%	0.70%	0.59%	0.50%
	$Q_{f,i}/\Delta H$	0.027%	0.034%	0.016%	0.049%	0.029%
3	$Q_{s,i}/\Delta H$	6.6%	5.4%	6.3%	6.1%	3.9%
	$Q_{p,i}/\Delta H$	0.038%	0.023%	0.032%	0.047%	0.024%

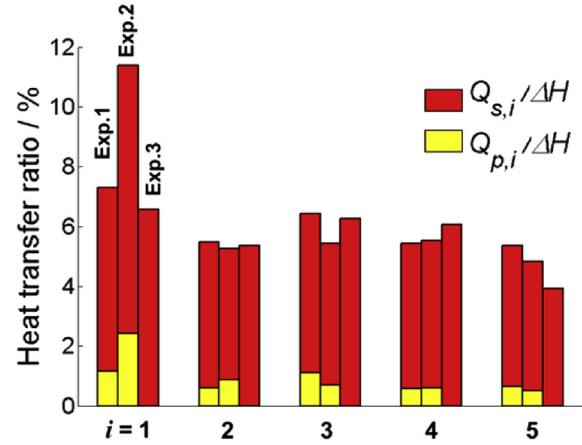


Fig. 16. Heat transfer ratio during penetration induced TR propagation test.

of the battery system above the batteries, because the temperature at the top of the flame can be much higher than that at the bottom.

Fig. 16 displays the normalized heat transfer ratios, $Q_{s,i}/\Delta H$, $Q_{p,i}/\Delta H$ in penetration induced TR propagation tests, and the data reveals that: 1) less than 12% of the total heat released in TR drove the TR propagation from Bat 1 to Bat 2. 2) It took even less than 7% of the total heat released for the TR to propagate from Bat i to Bat $i + 1$ for $i \in \{2, 3, 4, 5\}$. 3) The heat transfer through the pole connector accounted for 1% of ΔH for most of the cases, which is approximately 1/10 of the heat transferred through battery shell.

It is worth noting that the thermal resistance ratio R_p/R_s is approximately equal to 1, as calculated in Eq. (18), while the $Q_{p,i}/Q_{s,i}$ only approximates 1/10.

$$\frac{R_p}{R_s} = \frac{\lambda_s \cdot A_s}{\lambda_p \cdot A_p} = \frac{0.5 \times 0.01354}{146 \times 0.00004} = 1.16 \quad (18)$$

Mathematically, according to (14), the reason for the low value of heat transfer ratio $Q_{p,i}/Q_{s,i}$ is caused by the difference of TC_y and TC_z , or the difference in the temperature distribution as shown in Fig. 15. However, the heat flow is determined by the total thermal resistance between heat transfer nodes. Therefore the heat flow ratio $Q_{p,i}/Q_{s,i}$ equals to the ratio of the total thermal resistance as shown in Eq. (19), where R_{up} means the thermal resistance of the jelly roll towards the upside to the battery pole. In addition, the relative value of R_{up} can be acquired by Eq. (20), which will benefit future work of TR propagation modeling.

$$\frac{Q_{p,i}}{Q_{s,i}} = \frac{R_s}{R_p + 2 \cdot R_{up}} \approx \frac{1}{10} \quad (19)$$

$$\frac{R_{up}}{R_s} = \frac{1}{2} \cdot \left(\frac{Q_{s,i}}{Q_{p,i}} - \frac{R_p}{R_s} \right) \approx 4.4 \quad (20)$$

Moreover, there was no appreciable difference between results of the pack with connector (experiment No. 1 and 2) and without (experiment No. 3). Therefore more attention should be paid to the heat transfer path through the battery shell in seeking inhibition strategies to prevent TR propagation.

3.9. A look into the ashes

A closer look into the ashes resulting from the test could reveal insights for understanding the mechanisms of TR propagation and physical evidence to support the future modeling assumptions.

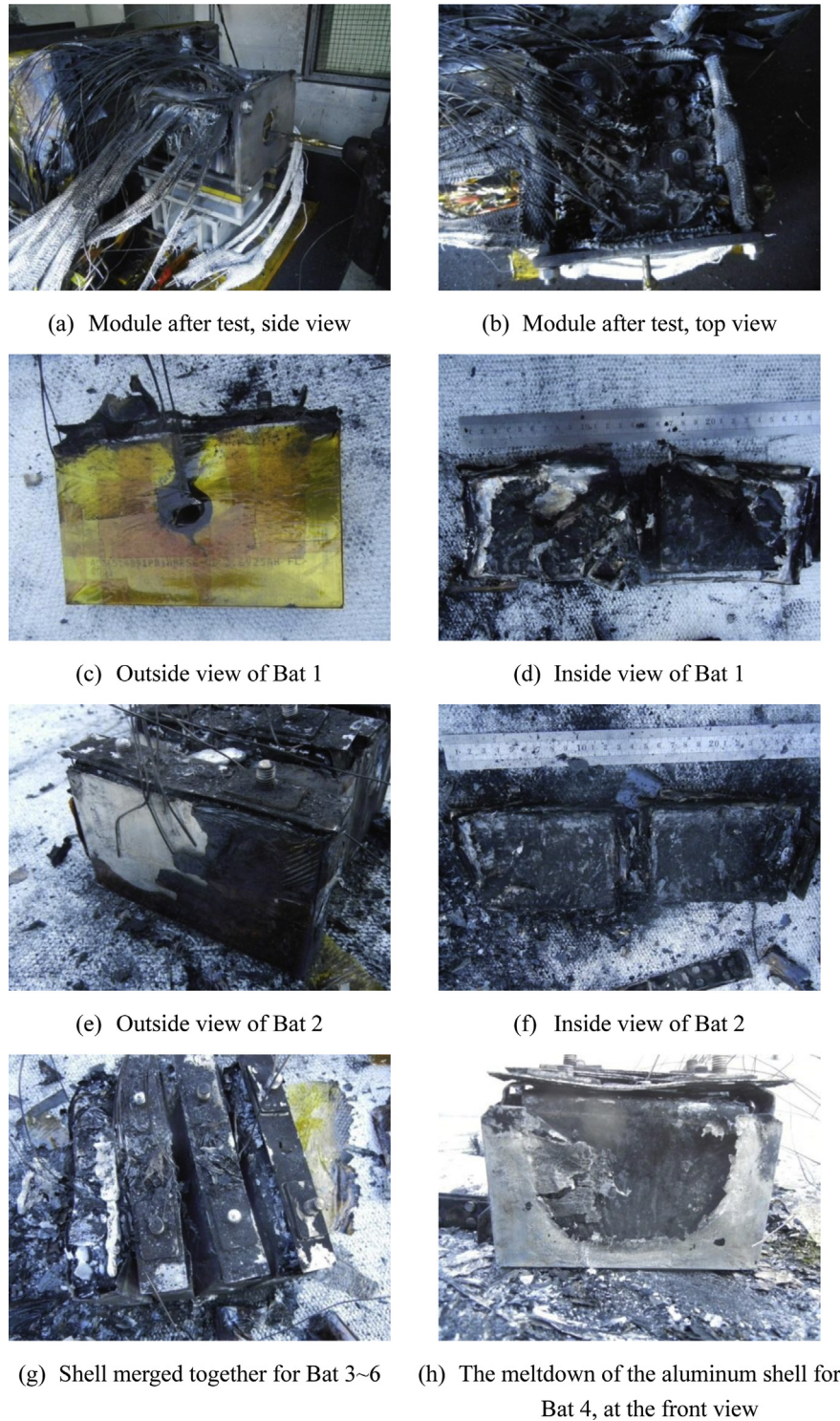


Fig. 17. A look into the ashes after a penetration induced TR propagation test.

Fig. 17 shows the residuals of the battery module after the penetration induced TR propagation test for experiment No. 2. Fig. 17a and b shows the status of the battery module after the penetration induced TR propagation test. Fig. 17c provides the view of Bat 1 from the direction where the nail came in. The yellow Kapton tape (in the web version), albeit shrunk, could be easily identified. Fig. 17d shows the middle layer between the two pouch cells of Bat 1. Some residuals of aluminum-plastic film of the pouch cell can be

seen at the edges, where the melting point of aluminum, $660\text{ }^{\circ}\text{C}$, was not reached. Fig. 17e provides the outside view of Bat 2 toward Bat 1. The missing of well-wrapped Kapton tape indicates that the temperature at the surface of Bat 2 was higher than that of Bat 1. Fig. 17f shows that almost no aluminum foils can be found at the core of Bat 2, indicating that the maximum temperature inside Bat 2 exceeded the melting point of aluminum at most positions. The shells of Bat 3–Bat 6 merged together due to the melting of the

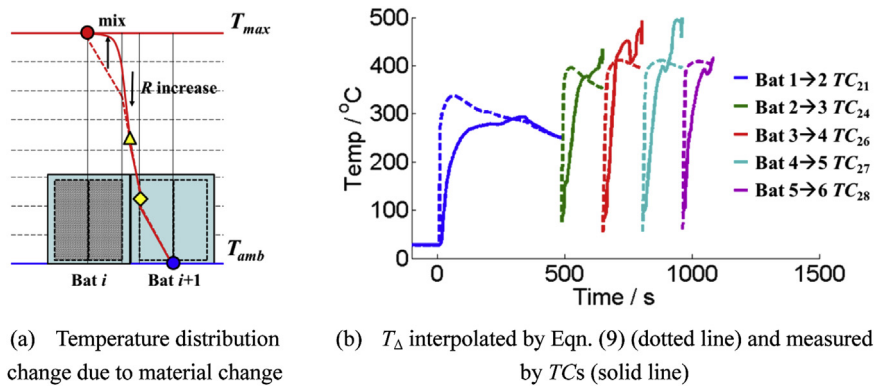


Fig. 18. Possible changes in the temperature distribution due to material damage during penetration induced TR propagation test.

aluminum shell of the batteries at extreme temperature, as seen in Fig. 17g. After separating Bat 3 from Bat 4, partial loss of the aluminum shell at the upper side of Bat 4 can be observed in Fig. 17h. The observations for the aluminum shell loss were similar for Bat 5 and 6. The melting of the aluminum shell suggests that the use of aluminum as the material of the battery shell might need to be reconsidered, given its poor protection of the battery jelly roll in TR condition.

3.10. A discussion on the material changes

The material inside the battery changed when TR happened. For one thing, the burst out gas carried some material away, resulting in loss of the battery mass. For another, high temperature changed the original materials and their thermal resistance inside the battery. Such a change may influence the heat transfer path through the battery shell. However, we expect that it would not change the heat transfer paths through the connector or by fire scorching, because the connector made by copper changed a little and the adjacent battery did not decompose before the onset of its own TR.

Fig. 18a illustrates possible changes in the temperature distribution due to material damage. The dotted line is for the assumption without material damage, while the solid line is for the condition with material damage. The mix of the materials leads to a higher temperature at the outside of the damaged jelly roll. However, the increase in thermal resistance makes the temperature drop steeper at the edge of the damaged jelly roll. Therefore the actual change in T_{Δ} , caused by material decomposition, is negligible for the battery under investigation, which can be verified by the results shown in Fig. 18b.

Fig. 18b shows that the measured T_{Δ} (solid line) and the calculated T_{Δ} (calculated by Eq. (9), dotted line) are similar. According to Eqs. (9), (10) and (14), the heat transfer through the battery shell can be calculated by Eq. (21), where αR_s denotes the thermal resistance between T_{Δ} and TC_{i+1} , which did not change before TR happens on Bat $i+1$. Therefore T_{Δ} dominates the heat transfer through the battery shell. In addition, the small difference between the measured and the calculated T_{Δ} confirms that the analysis in Sec. 3.8 for the heat transfer through the battery shell is reasonable without considering the material decomposition.

$$q_{s,i}(t) = \frac{TC_i(t) - TC_{i+1}(t)}{R_s} = \frac{TC_{\Delta}(t) - TC_{i+1}(t)}{\alpha R_s}, \quad \left(i \in \{1, 2, 3, 4, 5\} \right) \quad (21)$$

4. Conclusion

In this paper we have analyzed the mechanisms of a penetration-induced TR propagation within a large format lithium ion battery module based on experiment data. The TR was triggered by nail penetration of the first battery, followed by TR propagation to adjacent batteries. The experimental results lead to the following conclusions:

We have, for the first time, reported the temperature responses for a large format lithium ion battery module during a penetration induced TR propagation test. The onset temperature ($T_{\text{onset},i}$) at the battery core was lowered to 65–116 °C (compared to the EV-ARC test results in Ref. [36]) due to side heating in the TR propagation condition. TR will happen when the onset temperature measured in EV-ARC tests ($T_{\text{onset,ARC}}$) is reached at any point within the large format battery. In addition, the maximum temperature difference (MTD) within a battery can be as high as 593–792 °C during a penetration induced TR propagation test.

The heat transfer through the battery shell, through the pole connector as well as by the fire scorching on the cover of adjacent battery has been quantified. The investigation leads to the conclusion that the heat transferred through the battery shell dominates the heat transfer process. The fire has little influence on the TR propagation, but may cause significant damage on the accessories located above the battery module. Therefore more attention should be paid to find ways to prevent TR propagation through the battery shell, and protect the accessories from TR related fire hazards.

Our future work will focus on building a TR propagation model to study possible ways to prevent TR propagation in a large format lithium ion battery, and also on investigating the material properties of the battery after damaged by high temperature during TR.

Acknowledgment

This work is funded by US-China Clean Energy Research Center-Clean Vehicle Consortium (CERC-CVC), and the MOST (Ministry of Science and Technology) of China under the contract of No. 2014DFG71590, and also funded by BMW China Services Ltd.

The first author appreciates the substantial discussion with Mr. Caihao Weng from the University of Michigan, Ann Arbor and Mr. Mou Fang from Tsinghua University. The author would like to thank Mr. Maogang Li from Thermal Hazard Technology for supporting the EV-ARC.

The author would like to thank Mr. Mingxuan Zhang from Tsinghua University, and Mr. Bin Fan, Mr. Hongqing Wang, Mr. Qiang Liu, Mr. Guangli Bai, Mr. Tao Cheng, Mr. Xin He, Mr. Lei Liu,

Mr. Shiqiang Liu and Mr. Zhonghua Ma from CATARC for the experimental support of thermal runaway propagation.

References

- [1] Q.S. Wang, P. Ping, X. Zhao, et al., Thermal runaway caused fire and explosion of lithium ion battery, *J. Power Sources* 208 (2012) 210–224.
- [2] Garrett P. Beauregard, Report of Investigation: Hybrids Plus Plug in Hybrid Electric Vehicle, eTec, Phoenix AZ, 2008.
- [3] B. Smith, Chevrolet Volt Battery Incident Overview Report, U.S. Department of Transportation, National Highway Traffic Safety Administration, 2012, p. 1.
- [4] Case Number DCA13IA037, Interim Factual Report: Boeing 787-8, JA829J Battery Fire, National Transportation Safety Board, Office of Aviation Safety, Washington, DC, USA, 2013.
- [5] N. Willard, W. He, C. Hendricks, M. Pecht, Lessons learned from the 787 dreamliner issue on lithium-ion battery reliability, *Energies* 6 (2013) 4682–4695.
- [6] D.H. Doughty, Vehicle Battery Safety Roadmap Guidance, Oct. 2012.
- [7] J. Wen, Y. Yu, C. Chen, A review on lithium-ion batteries safety issues: existing problems and possible solutions, *Mater. Express* 2 (3) (2012) 197–212.
- [8] SAE J2464–J2009.
- [9] IEC-62133–2002.
- [10] Cindy Millsaps, Second Edition of IEC 62133: the standard for Secondary Cells and Batteries Containing Alkaline or other non-acid electrolytes is in its final review cycle, *Battery Power* 16 (3) (2012) 16–18. http://www.nxtbook.com/nxtbooks/webcom/batterypower_20120506/index.php?startid=16.
- [11] QCT 743–2006.
- [12] QCT 743-2012 (Revised edition calling for opinions).
- [13] SAE J1929–2011.
- [14] IEC 62660-2-2010.
- [15] UL 1642-2009.
- [16] UL 2054-2009.
- [17] UL 2580-2010.
- [18] ISO/WD 12405-2-2010.
- [19] JIS-C-8715-2-2012.
- [20] P. Ramadass, W. Fang, Z. Zhang, Study of internal short in a Li-ion cell I. Test method development using infra-red imaging technique, *J. Power Sources* 248 (2014) 769–776.
- [21] J. Lamb, C.J. Orendorff, Evaluation of mechanical abuse techniques in lithium ion batteries, *J. Power Sources* 247 (2014) 189–196.
- [22] W. Fang, P. Ramadass, Z. Zhang, Study of internal short in a Li-ion cell II. Numerical investigation using a 3D electrochemical-thermal model, *J. Power Sources* 248 (2014) 1090–1098.
- [23] S. Santhanagopalan, P. Ramadass, J. Zhang, Analysis of internal short-circuit in a lithium ion cell, *J. Power Sources* 194 (2009) 550–557.
- [24] M. Keyser, D. Long, J. Ireland, A. Pesaran, E. Darcy, M. Shoesmith, B. McCarthy, Internal short circuit instigator in lithium ion cells, in: Presentation in Battery Safety Conference 2013, San Diego, Nov. 14, 2013.
- [25] H. Maleki, J.N. Howard, Internal short circuit in Li-ion cells, *J. Power Sources* 191 (2009) 568–574.
- [26] Y. Yamauchi, K. Mizushima, Y. Satoh, S. Yamada, Development of a simulator for both property and safety of a lithium secondary battery, *J. Power Sources* 136 (2004) 99–107.
- [27] T.G. Zavalis, M. Behm, G. Lindbergh, Investigation of short-circuit scenarios in a lithium-ion battery cell, *J. Electrochem. Soc.* 159 (6) (2012) 848–859.
- [28] S. Liu, F. Wang, B. Fan, Z. Zhang, F. Pei, Influence of penetration speeds on power Li-ion-cell's safety performance, *J. Automot. Saf. Energy* 4 (1) (2013) 82–86.
- [29] R. Spotnitz, J. Weaver, G. Yeduvaka, et al., Simulation of abuse tolerance of lithium-ion battery packs, *J. Power Sources* 163 (2007) 1080–1086.
- [30] A. Smyshlyayev, M. Krstic, N. Chaturvedi, et al., PDE model for thermal dynamics of a large Li-ion battery pack, in: American Control Conference on O'Farrell Street, San Francisco, CA, USA, 2011, June 29–July 01, pp. 959–964.
- [31] J.A. Jeevarajan, Hazards associated with high voltage high capacity lithium-ion batteries, *ECS Trans.* 33 (22) (2011) 1–6.
- [32] K.J. Lee, K. Smith, A. Pesaran, et al., Three dimensional thermal-, electrical-, and electro chemical-coupled model for cylindrical wound large format lithium-ion batteries, *J. Power Sources* 241 (2013) 20–32.
- [33] G.H. Kim, A. Pesaran, R. Spotnitz, A three-dimensional thermal abuse model for lithium-ion cells, *J. Power Sources* 170 (2007) 476–489.
- [34] G. Guo, B. Long, B.G. Cao, et al., Three dimensional thermal finite element modeling of lithium-ion battery in thermal abuse application, *J. Power Sources* 195 (2010) 2393–2398.
- [35] C. Yang, G.H. Kim, S. Sathanagopalan, A. Pesaran, Multi-physics modeling of thermal runaway propagation in a battery module, in: Meeting Abstract, 223rd ECS Meeting, Orlando, FL, May 2014.
- [36] X. Feng, M. Fang, X. He, M. Ouyang, L. Lu, H. Wang, M. Zhang, Thermal runaway features of large format prismatic lithium ion battery using extended volume accelerating rate calorimetry, *J. Power Sources* 255 (2014) 294–301.
- [37] X. Feng, J. Sun, M. Ouyang, X. He, L. Lu, X. Han, M. Fang, H. Peng, Characterization of large format lithium ion battery exposed to extremely high temperature, *J. Power Sources* 272 (2014) 457–467.
- [38] H. Zheng, Q. Sun, G. Liu, X. Song, V.S. Battaglia, Correlation between dissolution behavior and electrochemical cycling performance for $\text{LiNi}_{1/3}\text{Co}_{1/3}\text{Mn}_{1/3}\text{O}_2$ -based cells, *J. Power Sources* 207 (2012) 134–140.
- [39] W. Liu, M. Wang, J. Chen, X. Zhang, H. Zhou, Synthesis of $\text{LiNi}_{0.5}\text{Co}_{0.2}\text{Mn}_{0.3}\text{O}_2$ for lithium ion batteries and the mechanism of capacity fading at high temperature, *J. Electrochem.* 18 (2) (2012) 118–124 (in Chinese).
- [40] S. Boyd, L. Vandenberghe, *Convex Optimization*, Cambridge University Press, 2004.
- [41] J. H. Lienhard IV and J. H. Lienhard V. *A heat transfer text book*, third edition. Phlogiston Press, Cambridge, Massachusetts, U.S.A. pp62–78.
- [42] Y. Fu, S. Lu, K. Li, C. Liu, X. Cheng, H. Zhang, An experimental study on burning behaviors of 18650 lithium ion batteries using a cone calorimeter, *J. Power Sources* 273 (2015) 216–222.
- [43] J. Zhang, B. Wu, Z. Li, J. Huang, Simultaneous estimation of thermal parameters for large-format laminated lithium ion batteries, *J. Power Sources* 259 (2014) 106–116.